Electronic Supplementary Information for

Structure-enabled Long-lived Charge Separation in Single Crystals of an Asymmetric Donor-Acceptor Perylenediimide Cyclophane

Malik L. Williams†, Adam F. Coleman†, Kathryn R. Peinkofer, Ryan M. Young*, and Michael R. Wasielewski*

Department of Chemistry and Paula M. Trienens Institute for Sustainability and Energy

Northwestern University, Evanston IL 60208-3113

† M.L.W. and A.F.C. contributed equally to this work.

*Address correspondence to these authors

Contents

1. Synthesis and characterization

Briefly, **tpPDA**,[1] **pyrPDA,**[2] and tert-butyl 4-(aminomethyl)benzylcarbamate[1] were prepared according to literature. **PyrPDI-tpPDI** was synthesized by condensing a mono-BOC protected *p*-xylylenediamine with **tpPDA**. The amine was then de-protected and reacted with the **pyrPDA** to form **pyrPDI-tpPDI**. tpPDA and pyrPDA were synthesized according to literature.[1, 3] *tert*-butyl 4-(aminomethyl)benzylcarbamate was made according to literature or purchased.

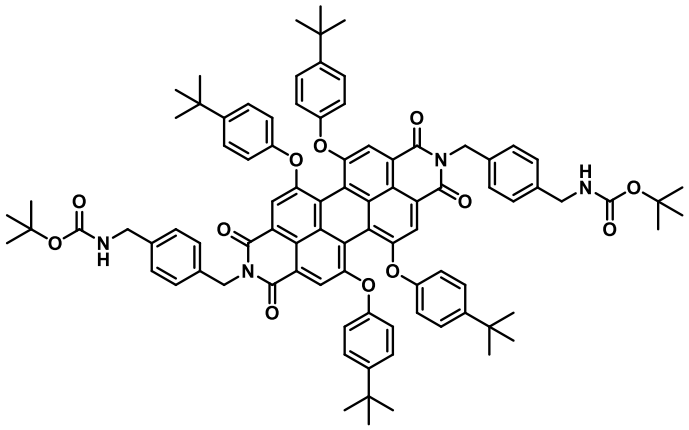

Synthesis of tpPDI with protected linker. 101mg (0.1 mmol) of tpPDA was mixed with 105mg (0.4 mmol) of tert-butyl 4-(aminomethyl)benzylcarbamate in toluene (20mL). The mixture was refluxed for 21 hours. After cooling to room temperature, the solution was washed with water, the organic layers were collected, and the solvent was removed under reduced pressure. The crude mixture was purified by column chromatography (silica, CH_2Cl_2/CH_3OH 99:1) yielding 97mg of tpPDI with linker (40%).

^{1}H-NMR (500 MHz, $CDCl_3$): δ = (s, 4H), 7.40 (d, J=8.1 Hz, 4H), 7.22 (d, J=8.7 Hz, 8H), 7.17 (d, J=7.5 Hz, 4H), 6.81 (d, J=8.7 Hz, 8H), 5.28 (s, 4H), 4.72 (bs, 2H), 4.23 (d, J=5.1 Hz, 4H), 1.42 (s, 18H), 1.28 (s, 36H) ppm.

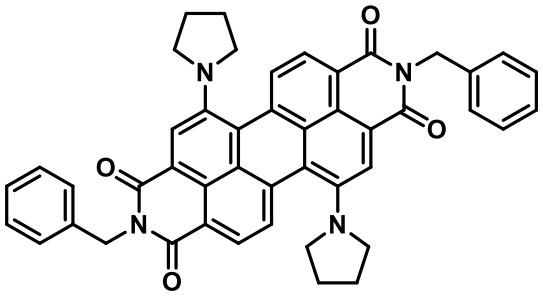

Synthesis of N,N-di(benzyl)-1,7-di(pyrrolidin-1′-yl)perylene-3,4,9,10-bis(dicarboximide). 1,7-di(pyrrolidin-1′-yl)perylene-3,4,9,10-tetracarboxy dianhydride (10mg, 19μmol), benzylamine (0.1mL, 0.9mmol), and dimethylacetamide (1mL) were mixed in a sealed 10mL round bottom flask. The flask was evacuated and back filled with nitrogen three times before heating to 110°C for 18 hours. After cooling to room temperature, 9mL of water was added, the solution was filtered, and the precipitate was collected. The crude product was purified via column chromatography (EtOAc/CH_2Cl_2 1:99, silica).

^{1}H-NMR (500 MHz, $CDCl_3$): δ = 8.52 (s, 2H), 8.46 (d, J=8.1 Hz, 2H), 7.73 (d, J=8.1 Hz, 2H), 7.55 (d, J=7.4 Hz, 4H), 7.33-7.28 (m, 4H), 7.25-7.21 (m, 2H), 5.43 (s, 4H), 3.82-3.67 (m, 4H), 2.90-2.75 (m, 4H), 2.14-1.90 (m, 8H) ppm.

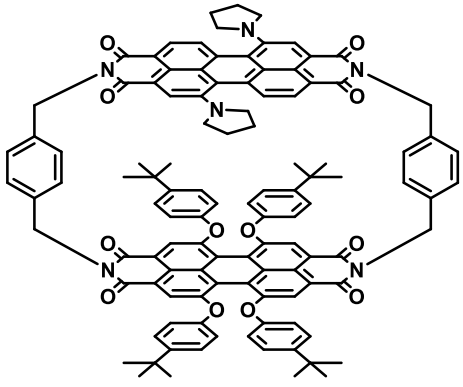

Synthesis of pyrPDI-tpPDI. 97mg (68 μmol) of tpPDI with linker was dissolved in 20mL of CH_2Cl_2. To this solution 1.3mL of TFA was added. The mixture was stirred under nitrogen for 2 hours. The solvent and TFA were removed under reduced pressure. The remaining solid was

then taken in a small amount of toluene and added to 36mg (68 µmol) of 1,7-dipyrrolidinylperylene-3,4,9,10-tetracarboxy dianhydride. An additional 200mL of toluene, 12mL of pyridine, and 1.2g of imidazole were then added, and the mixture was refluxed for 17 hours. The mixture was washed with water and the aqueous layers were subsequently extracted with CH_2Cl_2. The organic layers were combined, and the solvent removed under reduced pressure. The crude product was purified by column chromatography (CH_2Cl_2, silica) and HPLC, yielding 10mg of product (8%).

^{1}H-NMR (400 MHz, 353K, $C_2D_2Cl_4$): δ = 8.44 (s, 2H), 8.29 (d, J = 8.1 Hz, 2H), 8.08 (d, J = 10.8 Hz, 4H), 7.54 (d, J = 8.1 Hz, 2H), 7.48 (d, J = 8.1 Hz, 4H), 7.34 (d, J = 8.1 Hz, 4H), 7.21 (d, J = 9.0 Hz, 8H), 6.74 (d, J = 8.2 Hz, 8H), 5.52 (d, J = 13.0 Hz, 2H), 5.35 (bs, 2H), 5.21 (d, J = 13.6 Hz, 4H), 3.69 (d, J = 8.5 Hz, 4H), 2.18 (bs, 4H), 1.96 (bs, 4H), 1.34 (s, 36H).

HRMS (APCI, negative mode, DCM): *m*/*z*: calculated for $C_{112}H_{94}N_6O_{12}$: 1714.6930 $[M-H]^-$, found: 1714.6947.

2. Crystal growth and structure determination.

Single crystals of **pyrPDI-tpPDI** were grown by slow vapor diffusion of methanol into a solution prepared in toluene over the course of 3-4 weeks. A suitable crystal was selected and mounted on a loop using paratone oil. The crystal was cooled and kept at 100K during data collection, x-ray data was collected on a XtaLAB Synergy diffractometer using Cu Kα radiation. Using Olex2[4, 5], the structure was solved with the XT structure solution program using intrinsic phasing and refined with the XL refinement package using least squares minimization. The **pyrPDI-tpPDI** single crystal structure has been deposited in the Cambridge Crystallographic Data Centre database (CCDC #2342829). Additional single crystal structural data and synthesis details are reported in the Supporting Information. Crystals grown using the same conditions as above were dropped cast onto a clean glass slide and were used in optical experiments.

Intensity data of a purple plate-like single crystal of pyrPDI-tpPDI were collected at 100 K. A suitable single crystal with dimensions of 0.3 × 0.222 × 0.126 mm^3 was mounted on a MiTeGen loop with paratone oil on an XtaLAB Synergy diffractometer equipped with a micro-focus sealed X-ray tube PhotonJet (Cu) X-ray source and a Hybrid Pixel Array Detector (HyPix) detector. The temperature of the crystal was controlled with an Oxford Cryosystems low-temperature device. Data reduction was performed with the CrysAlisPro software using an empirical absorption correction. The structure was solved with the ShelXT structure solution program using the Intrinsic Phasing solution method and by using Olex2 as the graphical interface. The model was refined with ShelXL using least squares minimization. The structure was deposited in the Cambridge Crystallographic Data Center (CCDC #2342829).

Table S1. Crystal data and structure refinement for pyrPDI-tpPDI

Identification code	pyrPDI-tpPDI
Empirical formula	$C_{133}H_{115}N_6O_{12}$
Formula weight	1989.30
Temperature/K	100.01(10)
Crystal system	monoclinic
Space group	$P2_1/n$
a/Å	22.4426(12)
b/Å	20.9039(10)
c/Å	30.0536(10)
α/°	90
β/°	96.666(4)
γ/°	90
Volume/$Å^3$	14004.0(11)
Z	4
$\rho_{calc}g/cm^3$	0.944
μ/mm^{-1}	0.478
F(000)	4204.0
Crystal size/mm^3	0.3 × 0.222 × 0.126
Radiation	Cu Kα (λ = 1.54184)
2Θ range for data collection/°	6.716 to 110.19
Index ranges	$-23 \leq h \leq 23$, $-21 \leq k \leq 22$, $-27 \leq l \leq 31$
Reflections collected	71366
Independent reflections	17628 [R_{int} = 0.0460, R_{sigma} = 0.0390]
Data/restraints/parameters	17628/1633/1440
Goodness-of-fit on F^2	1.302
Final R indexes [I>=2σ (I)]	R_1 = 0.1055, wR_2 = 0.3262
Final R indexes [all data]	R_1 = 0.1341, wR_2 = 0.3502
Largest diff. peak/hole / e $Å^{-3}$	0.80/-0.41

3. Steady-state absorption and emission spectroscopy

Solution-phase absorption spectra were acquired in a variety of solvents on a Shimadzu UV1800 absorption spectrometer. Solution emission spectra were collected using a Horiba Nanolog spectrofluorimeter. The visible absorption spectra of the single crystals were obtained using a lab-built microspectrophotometer. The beam from a xenon arc lamp (Oriel Instruments, model 66902) was spatially filtered through a pinhole and polarized by using a Glan–Thompson polarizer. A motorized (ELL14K, Thorlabs) achromatic half-wave plate (SAQWP05M-700, Thorlabs) was used to rotate the linear polarization. The beam was then sent into the back port of an upright microscope (Eclipse Ti-U, Nikon). The beam was directed using an internal mirror of the microscope to a 20× reflective objective lens (LMM15X, Thorlabs) to focus the light on the sample. Light transmitted through the crystal was collected using a second objective lens and then sent to a lab-built monochromator (Richardson Gratings, 52A15BK-224C) and focused onto a fast line-scan camera (OctoPlus, Teledyne e2v), sampling at 100000 lines/s. For absorption measurements, a reference spectrum (on bare glass) and a transmission spectrum (through a single cocrystal) were collected for each polarization in the range 0–360° in 10° steps. A dark spectrum with no light on the sample was subtracted from all reference and transmission spectra.

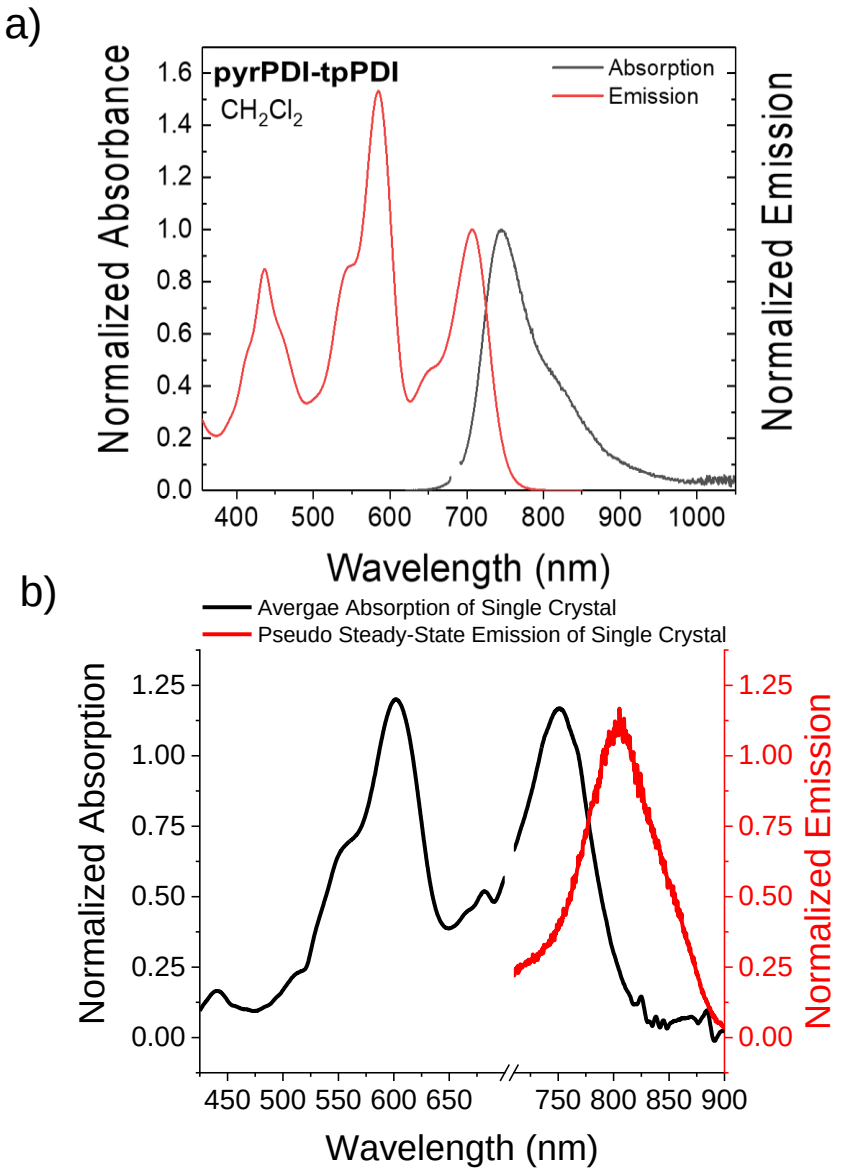

Figure S1. a) Normalized absorption and emission spectra for **pyrPDI-tpPDI** in CH_2Cl_2. b) Polarization-averaged steady-state absorption of a **pyrPDI-tpPDI** single-crystal from 0° to 360° and a pseudosteady-state emission spectrum acquired from the time integrated TRFM spectra.

4. Time-resolved spectroscopy

The femtosecond transient absorption (TA) experiments were conducted using instruments described previously.[6] The 700 nm pump pulses were generated using a laboratory-built collinear optical parametric amplifier and attenuated to 1 μJ/pulse. The pump pulses were depolarized to suppress the effects of orientational dynamics. Transient absorption spectra were detected using a customized Helios/EOS spectrometer (Ultrafast Systems, LLC). The optical density of the samples was ~0.5 at the excitation wavelength in 2 mm cuvettes.

Broad bandwidth excitation TA experiments to measure the ultrafast energy transfer process were conducted using an apparatus previously described.[7] Briefly, the 1040 nm fundamental output of a Yb:KGW regenerative amplifier system at 100 kHz (Spirit 1040-4, Spectra Physics, Inc.) seeded a noncollinear optical parametric amplifier (Spirit-NOPA, Light Conversion Inc.) to produce femtosecond pump pulses. These pulses were compressed using an acousto-optic modulator (AOM)-based pulse shaper. Second and third-order dispersion correction parameters were determined via maximizing second harmonic generation signal from a BBO crystal at the sample position. The pump pulses were centered at ~585 nm and focused on the sample along with a white light probe pulse. The pump and probe were parallel in polarization.

For the single crystals, the 1040 nm output from a commercial Yb:KGW, 4 W, 100 kHz repetition rate, 300 fs amplified laser system (Spirit-One, Spectra-Physics) was divided into two beams.[8] One beam was sent to an optical parametric amplifier (Spirit-OPA-8, Light Conversion) to generate the pump beam wavelengths. The pump was directed into an optical chopper (SR542, Stanford Research Systems), which was phase-synchronized to the laser output to modulate the beam at 12.5 kHz. The other 1040 nm beam was sent to a double-pass linear delay line (Newport, IMS600LM) and then focused into an 8 mm thick undoped YAG crystal for white light continuum generation. The beam was then recollimated, and the

fundamental was removed using a 1000 nm short-pass filter. The pump and probe beams were coaxially combined using a 50:50 beamsplitter and sent into the microscope system and spectrometer described above. The polarizations of the pump and probe beams were varied independently using two achromatic half-wave plates. The pump and probe power on the sample were each set to 2 μW by using two neutral density filters. The pump and probe focused spot size (4 standard deviations of a Gaussian, or 95% of the beam intensity) on the sample were 2.9 μm, giving pump and probe fluence of 0.6 mJ/cm^2 and 0.3 mJ/cm^2, respectively. To further mitigate systematic baseline shifts during the measurement, the TA spectrum at each delay point was individually referenced to a fixed negative delay point (−10 ps). The TA data for each cocrystal were chirp-corrected in lab-written Python software by fitting time-zero to a third-order polynomial.

Picosecond TRF data were collected using a commercial direct-diode-pumped 100 kHz Yb:KGW amplifier (Spirit 1040-HE, Spectra-Physics), producing a fundamental beam of 1040 nm (350 fs, 12 W), which was attenuated and used to pump a noncollinear optical parametric amplifier (Spirit-NOPA, Spectra-Physics) capable of delivering tunable, high-repetition-rate pulses with pulse durations as short as sub-20 fs. The samples were excited with 650 nm pulses attenuated to ~1 nJ/pulse. Fluorescence was detected using a Hamamatsu C4780 streak scope, as previously described. Samples were prepared in 1 mm pathlength quartz cuvettes. Time-resolved fluorescence microscopy (TRFM) data on single crystals of **pyrPDI-tpPDI** were collected using the same experimental setup outfitted with a commercial confocal microscope. The excitation pulses were tuned to 520 nm and attenuated to ~300 pJ/pulse to minimize scatter, with an excitation density of ~0.2 μJ/pulse. All data were acquired in the single-photon-counting mode using the Hamamatsu HPD-TA software. The temporal resolution, given by the instrument response function (IRF), was approximately 3% of the sweep window, with the shortest time resolution being ~30 ps.

Femtosecond Transient Absorption Spectroscopy Data

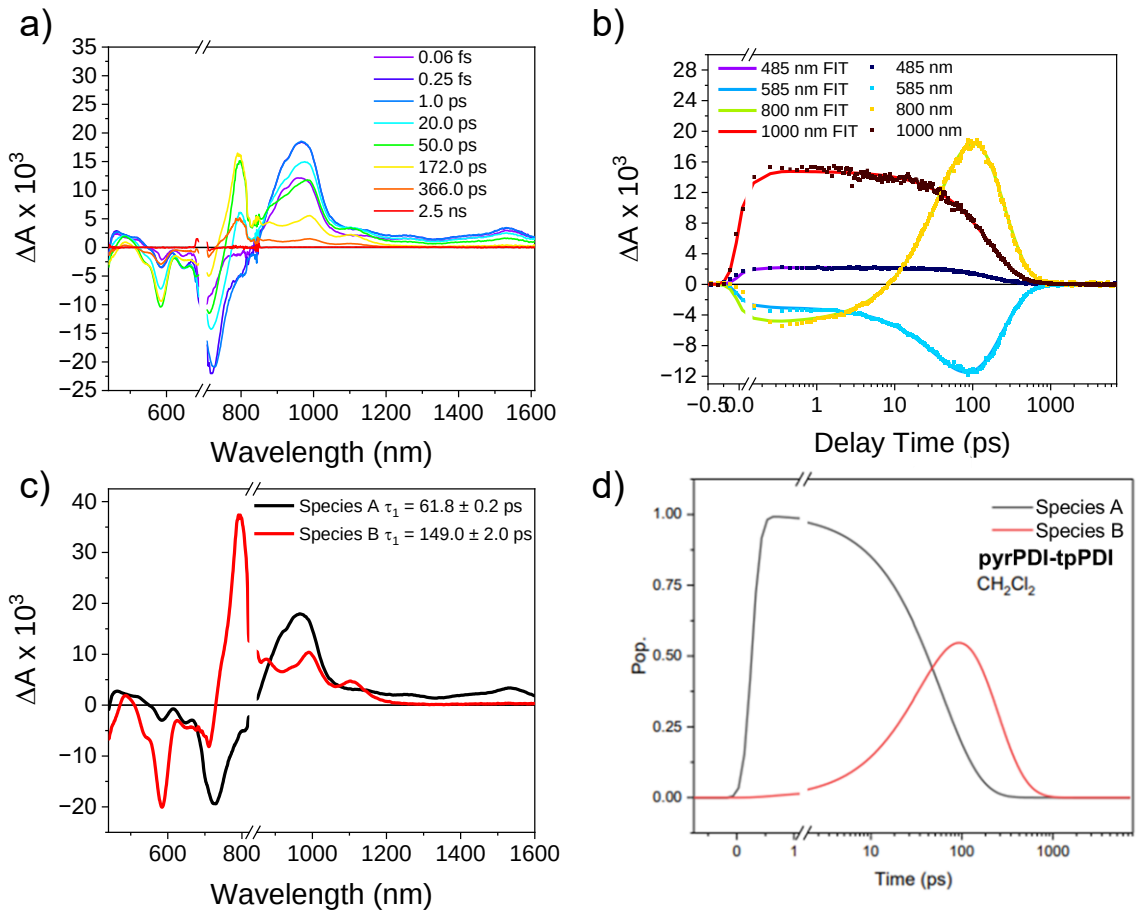

Figure S2. fsTA spectra of a) **pyrPDI-tpPDI** in CH_2Cl_2 at 298 K, λ_{ex} = 700 nm. b) Global fits to selected fsTA wavelengths to a sequential A → B → ground state kinetic model. Fits are shown as solid lines. c) Evolution-associated spectra obtained from deconvolution of the data set with the kinetic fit solution. Species A represents the S_1 state, and species B is the charge separated state. d) Solution to the kinetic model using the fit parameters.

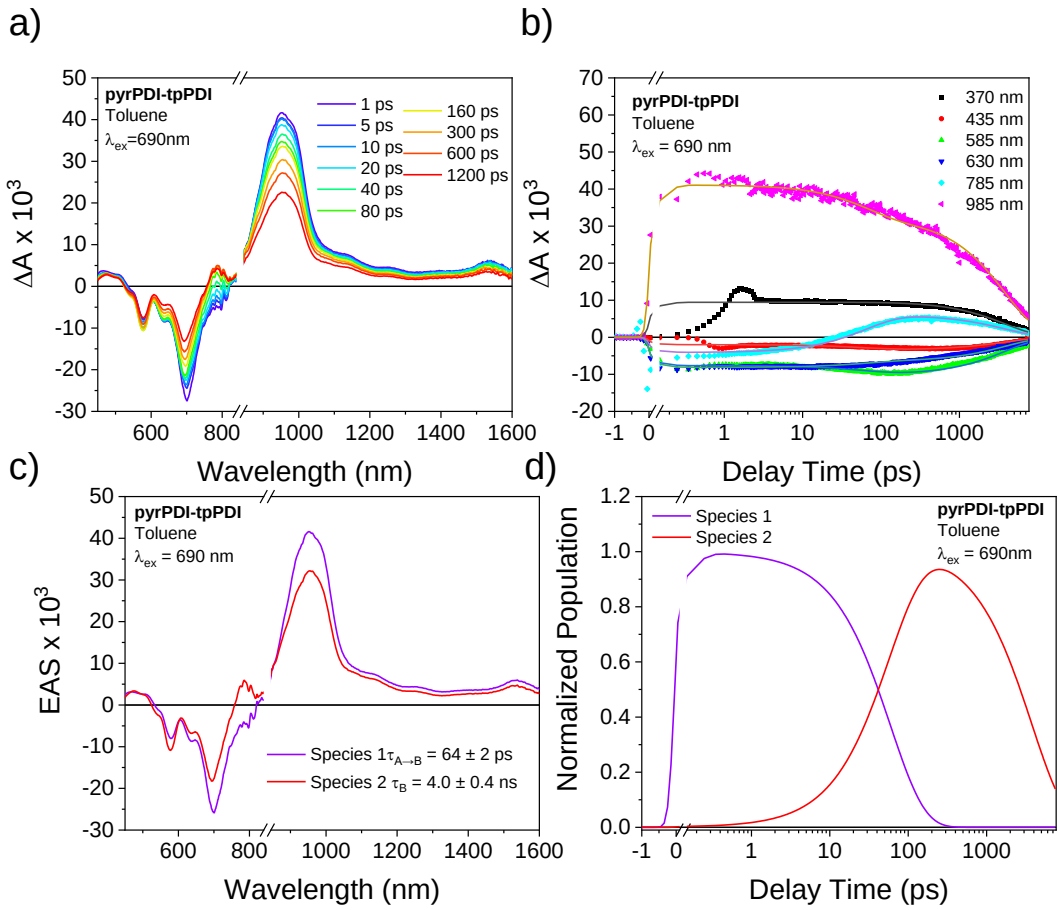

Figure S3. fsTA spectra of a) **pyrPDI-tpPDI** in toluene at 298 K, λ_{ex} = 690 nm. b) Global fits to selected fsTA wavelengths to a sequential A → B → ground state kinetic model. Fits are shown as solid lines. c) Evolution-associated spectra obtained from deconvolution of the data set with the kinetic fit solution. Species A represents the S_1 state, and species B is the partial charge separated state. d) Solution to the kinetic model using the fit parameters.

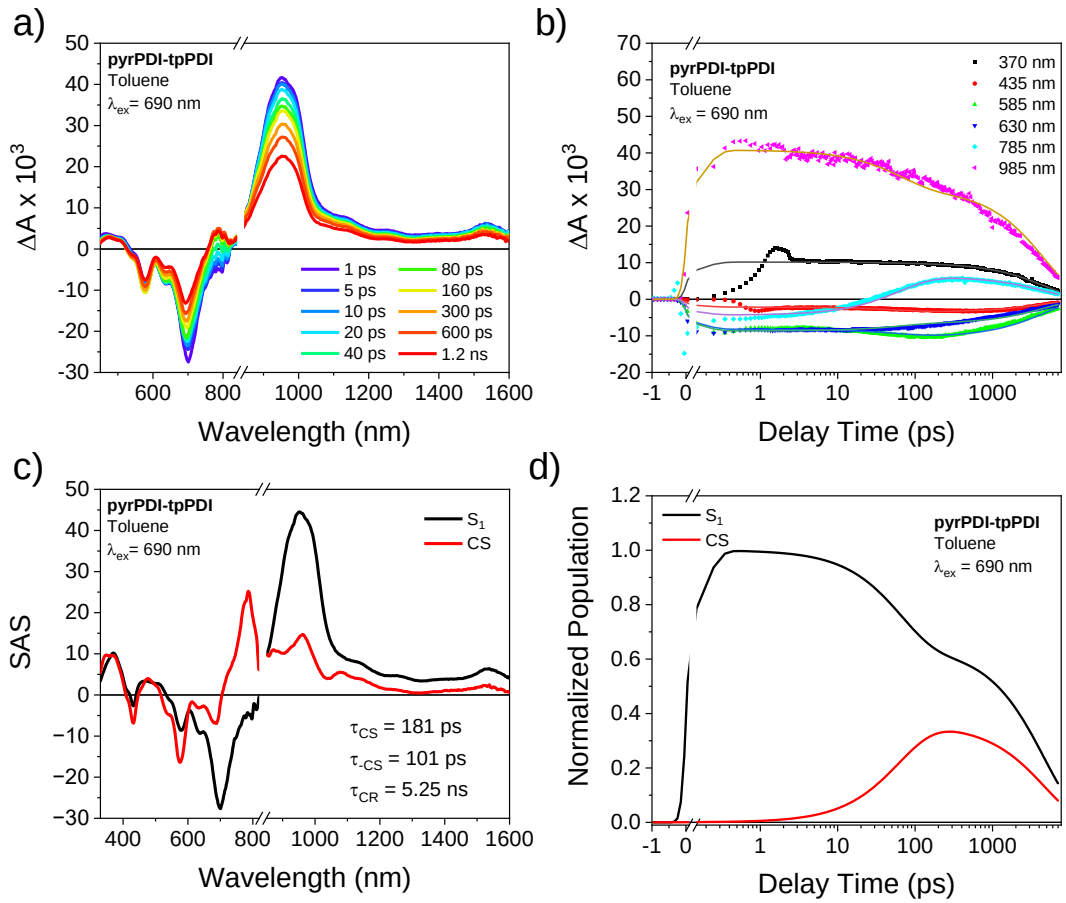

Figure S4. fsTA spectra of a) **pyrPDI-tpPDI** in toluene at 298 K, λ_{ex} = 690 nm. b) Global fits to selected fsTA wavelengths to an equilibrium model A ↔ B → ground state kinetic model. Fits are shown as solid lines. c) Evolution-associated spectra obtained from deconvolution of the data set with the kinetic fit solution. Species A represents the S_1 state, and species B is the charge separated state. d) Solution to the kinetic model using the fit parameters.

Nanosecond Transient Absorption Spectroscopy Data.

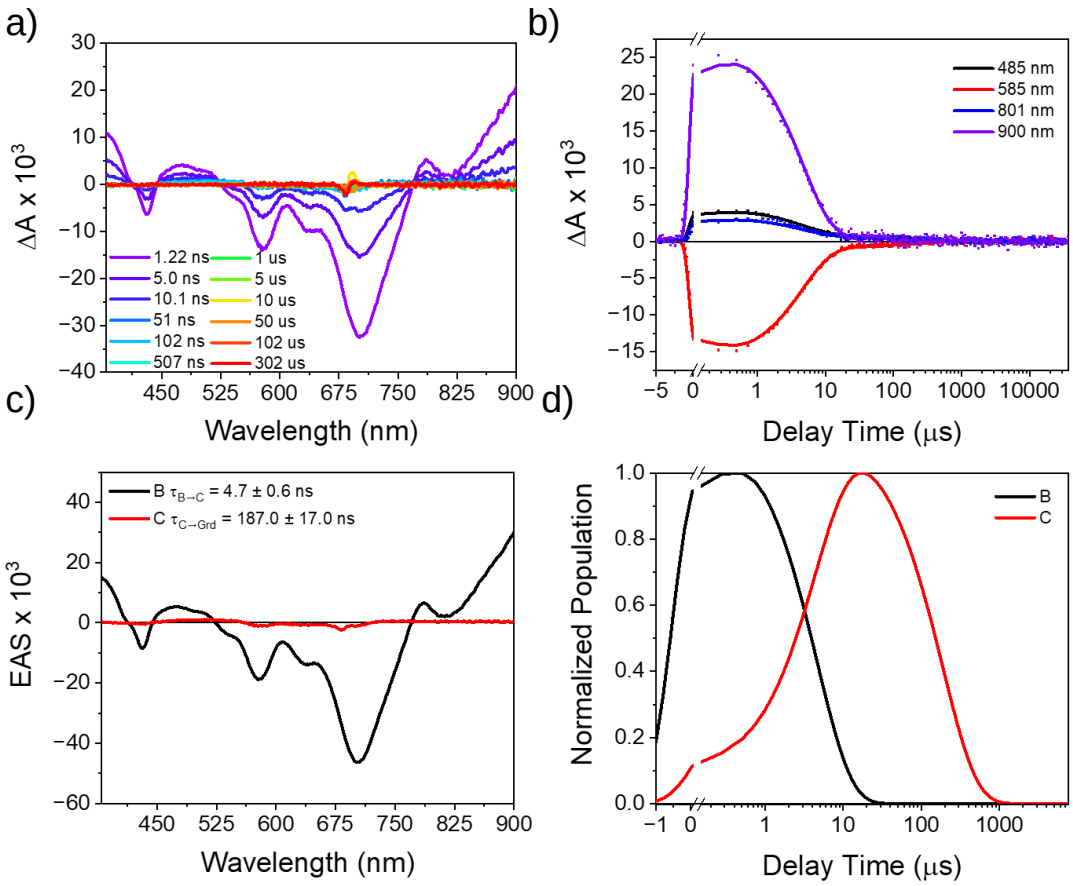

Figure S5. NsTA spectra of a) **pyrPDI-tpPDI** in toluene at 298 K, λ_{ex} = 690 nm. b) Global fits to selected nsTA wavelengths to a sequential B → C → ground state kinetic model. Fits are shown as solid lines. c) Evolution-associated spectra obtained from deconvolution of the data set with the kinetic fit solution. Species B represents the pseudo-equilibrium S_1-CS state and species C is the **tpPDI** triplet state. d) Solution to the kinetic model using the fit parameters.

Broadband Transient Absorption Spectroscopy Data.

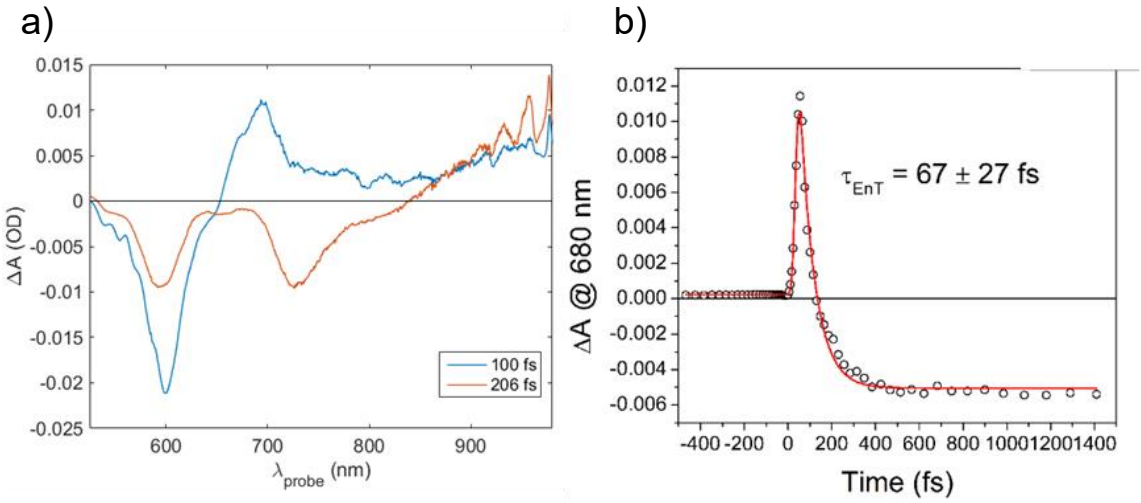

Figure S6. Selected broadband fsTA spectra of a) **pyrPDI-tpPDI** in CH_2Cl_2 at 298 K, λ_{ex} = 585 nm. b) Single wavelength exponential fit to 680 nm kinetic trace. Fit is shown as solid line.

Femtosecond Transient Absorption Microscopy Data.

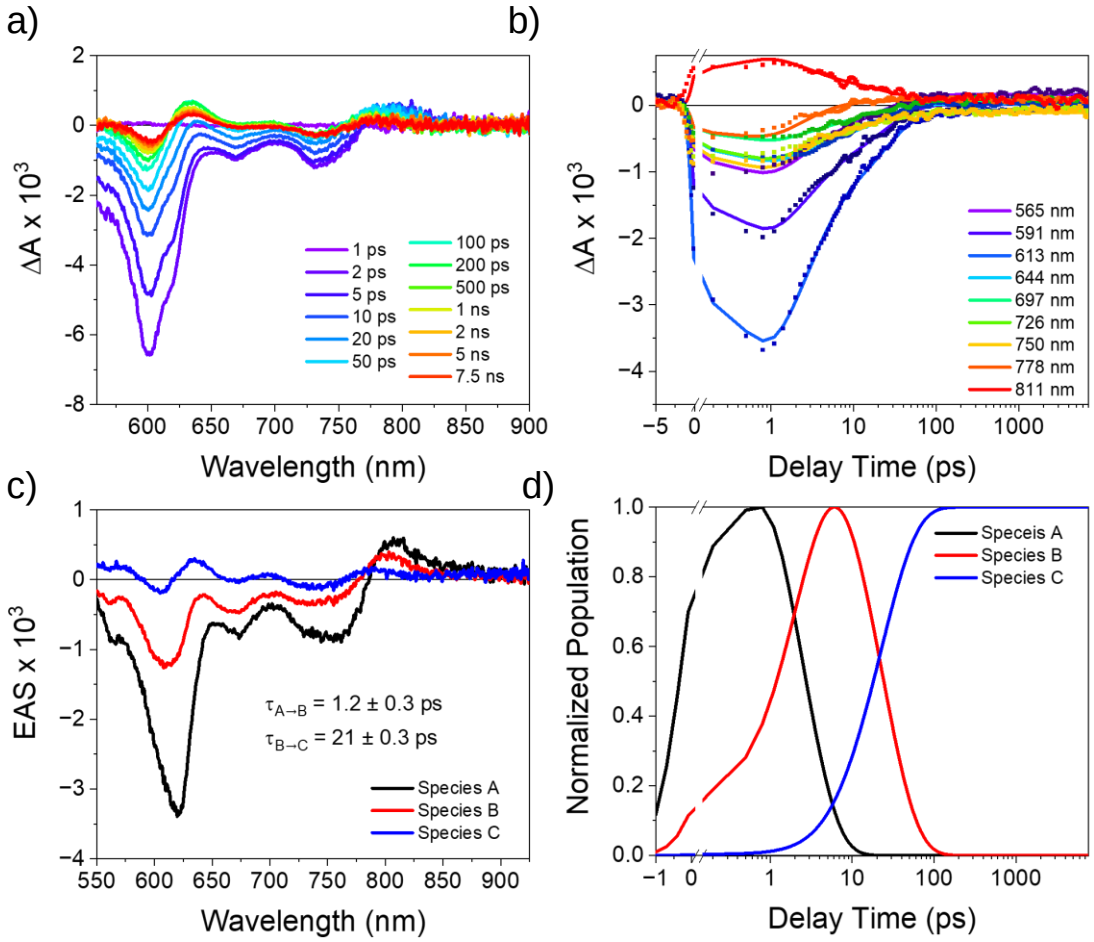

Figure S7. fsTAM spectra of a) **pyrPDI-tpPDI** single crystal at 298 K, λ_{ex} = 520 nm. b) Global fits to selected fsTAM wavelengths to a sequential A → B → C kinetic model. Evolution-associated spectra obtained from deconvolution of the data set with the kinetic fit solution. Species A represents the unrelaxed S_1 state, species B is relaxed S_1 state, and species C is the charge-separated state c) Global fits to selected fsTAM wavelengths. d) Solution to the kinetic model using the fit parameters.

Nanosecond Transient Absorption Microscopy Data.

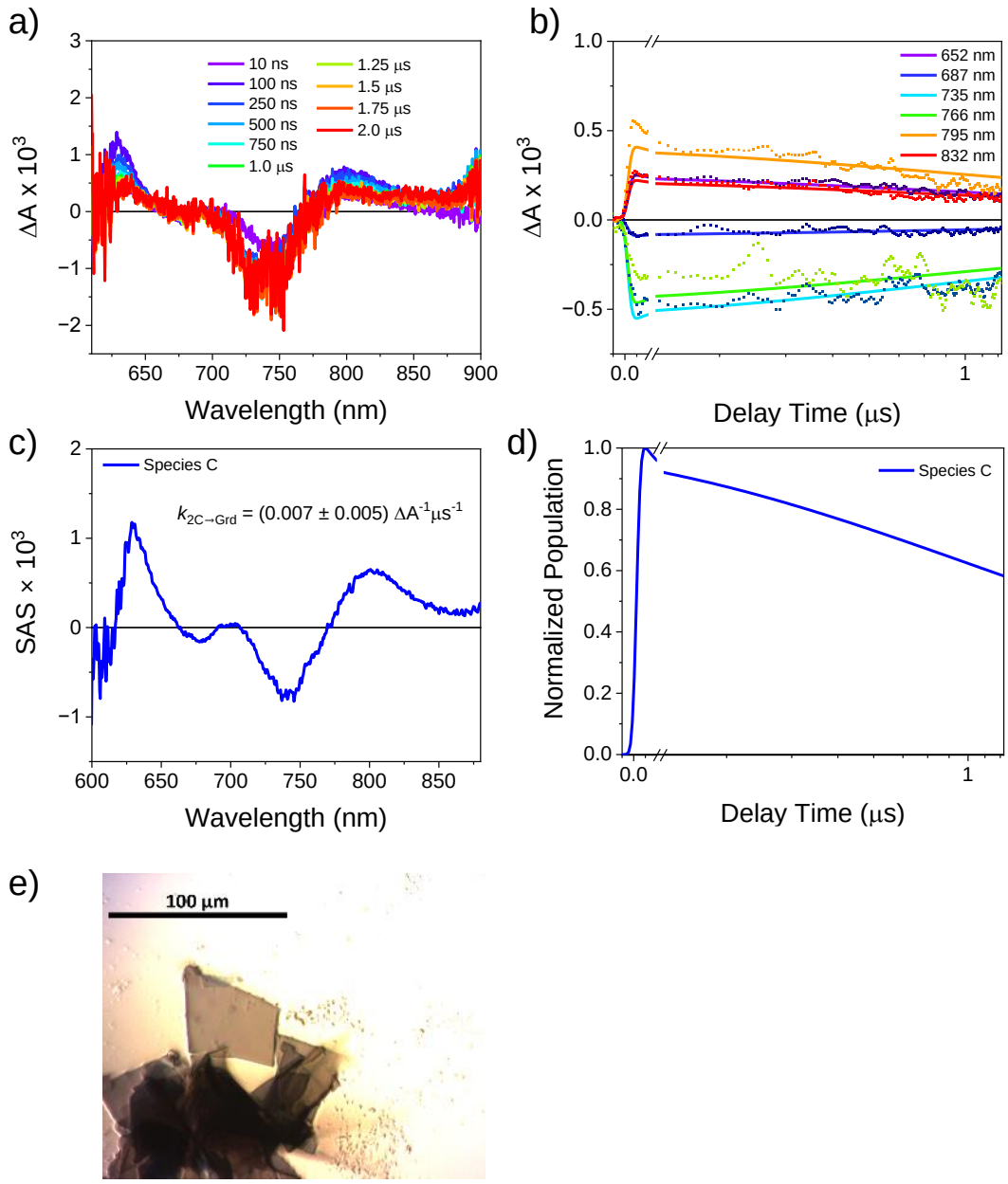

Figure S8. nsTAM spectra of a) **pyrPDI-tpPDI** single crystal at 298 K, λ_{ex} = 520 nm. b) Global fits to selected nsTAM wavelengths to a biomolecular one-dimensional singlet-singlet annihilation model, 2C → ground state kinetic model. c) Species-associated spectra obtained from deconvolution of the data set with the kinetic fit solution. d) Solution to the kinetic model using the fit parameters. E) optical micrograph of the crystal measured.

4. Time-Resolved Fluorescence Spectroscopy and Microscopy

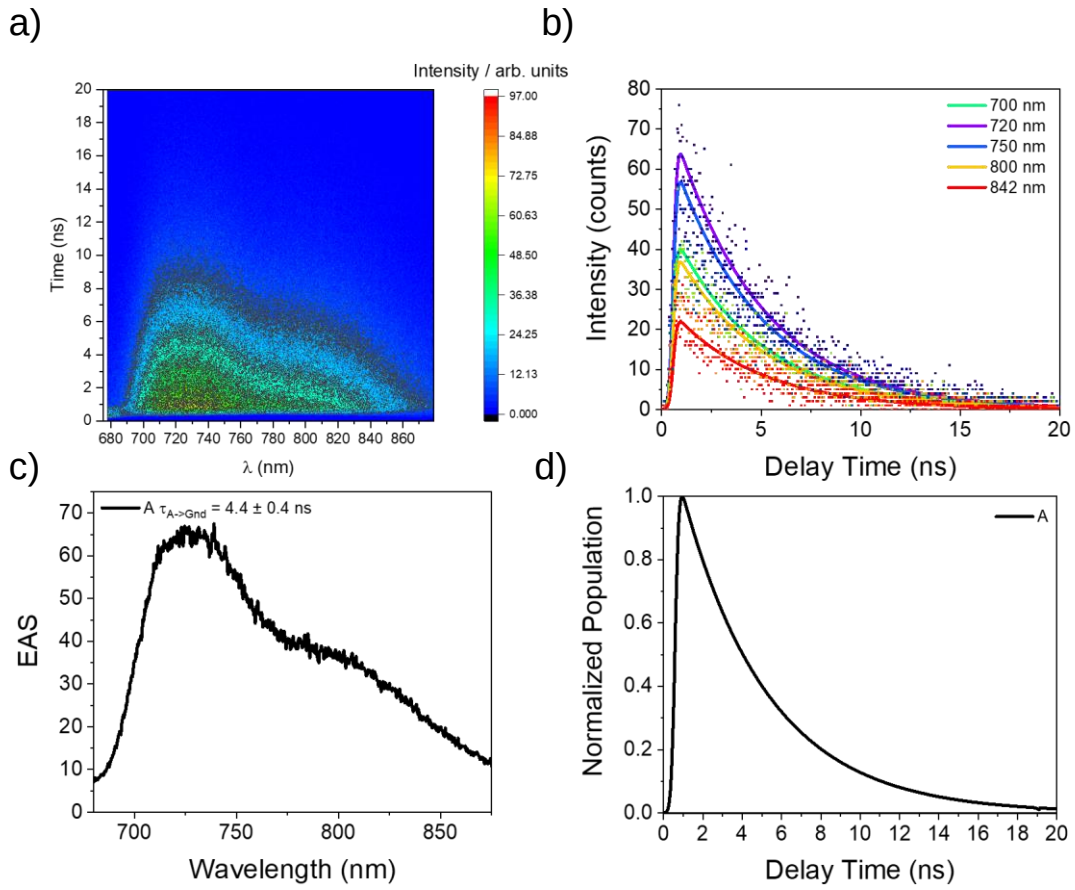

Figure S9. a) Time-resolved fluorescence data for the **pyrPDI** monomer in toluene, λ_{exc}= 650 nm in a 20 ns window. b) Kinetics at several wavelengths fit to a sequential A → Ground State model. c) Evolution-associated spectra. d) Model populations as functions of time.

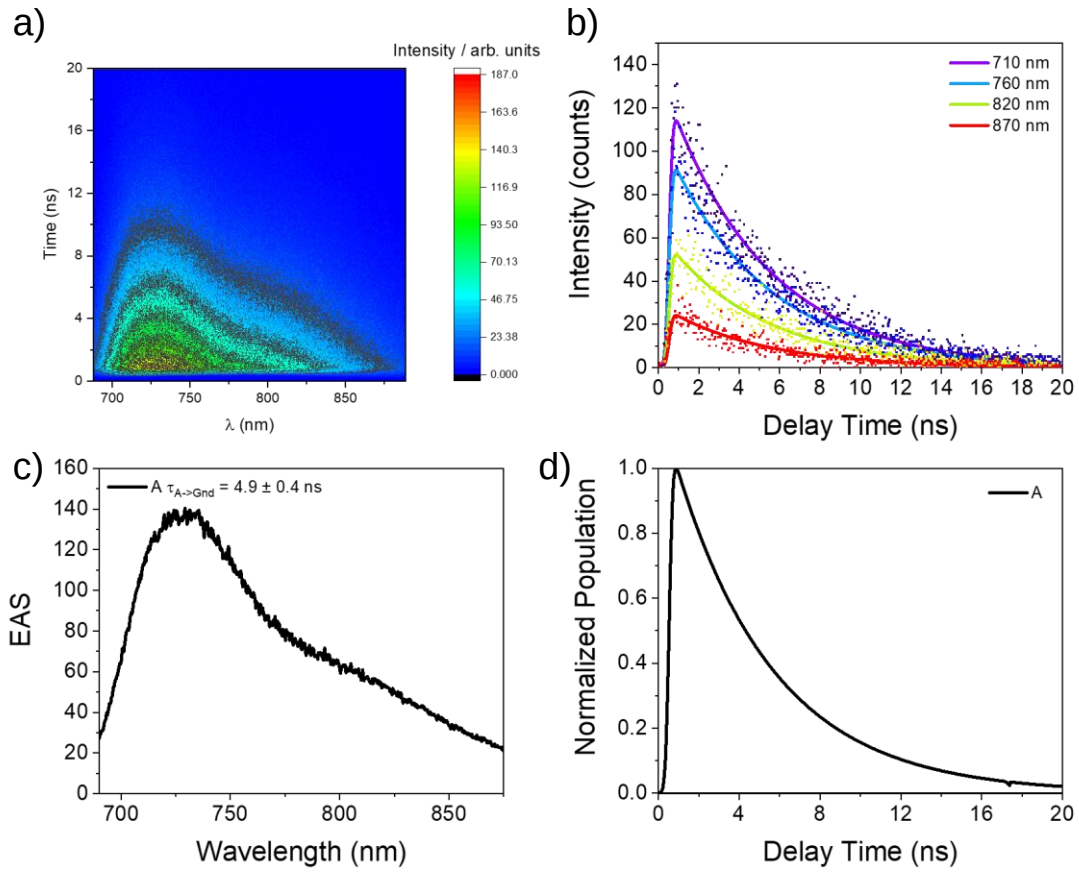

Figure S10. a) Time-resolved fluorescence data for the **pyrPDI-tpPDI** in toluene, λ_{exc}= 650 nm in a 20 ns window. b) Kinetics at several wavelengths fit to a sequential A → Ground state model. b) Evolution-associated spectra. d) Model populations as functions of time.

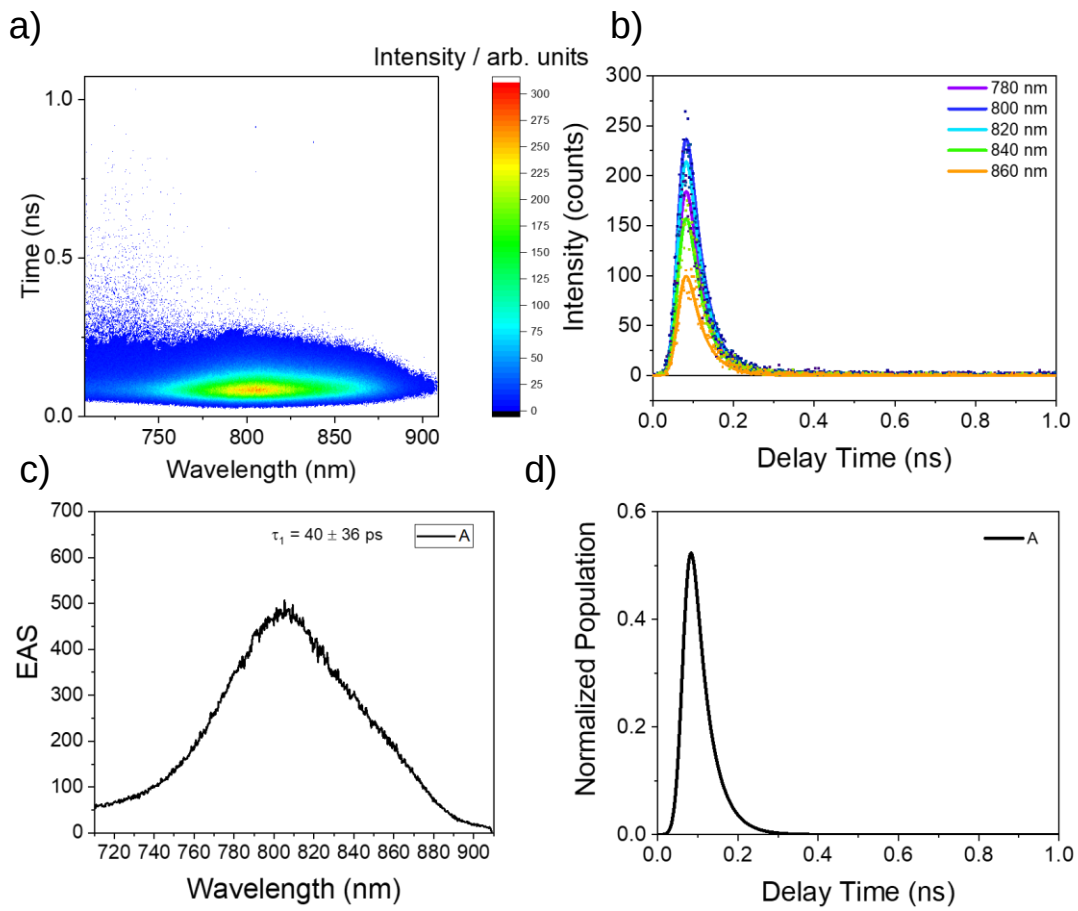

Figure S11. a) Time-resolved fluorescence data for the **pyrPDI-tpPDI** single crystal, λ_{exc} = 520 nm in a 1 ns window. b) Kinetics at several wavelengths fit to a sequential A → Ground state model. c) Evolution-associated spectra. d) Model populations as functions of time.

5. Kinetic Analysis

The fsTA data sets were globally analyzed using the kinetic rate matrix in equation S1 to extract their evolution-associated spectra and rate constants. These rate constants are used as inputs for the equilibrium-based species-associated analysis described below:

$$\begin{bmatrix} -k_A & 0 \\ k_A & -k_B \end{bmatrix} \quad \text{(Eq. S1)}$$

The eigenvalues of this matrix are $\lambda_1 = k_A$ and $\lambda_2 = k_B$ and can be used to find the rate constants of the full kinetic scheme. The kinetics involving the equilibrium between the excited state and CS state can be described by the following kinetic rate matrix:

$$\begin{bmatrix} -k_{IC} - k_f - k_{CS} & k_{-CS} \\ k_{CS} & -k_{-CS} - k_{CR} \end{bmatrix} \quad \text{(Eq. S2)}$$

Where the intrinsic S_1 decay including of fluorescence (*f*) and internal conversion (*IC*) contributions are taken from monomeric **pyrPDI** in toluene,[2] k_{CS} and k_{-CS} represent the forward and backward CS process, and k_{CR} is the charge recombination rate constant. The eigenvalues of this rate matrix are functions of the observed rate constants of S1. Along with the values of k_f and k_{IC}, we use the fluorescence quantum yield (Φ_f) of **pyrPDI** to constrain the model based on the derived expression for the quantum yield:

$$\Phi_f = \frac{k_f(k_{-CS} + k_{CR})}{(k_{IC} + k_f + k_{CS})(k_{-CS} + k_{CR}) - k_{CS}k_{-CS}} \quad \text{(Eq. S3)}$$

From these equations we can derive expressions for the other individual rate constants:

$$k_{CS} = \lambda_1 + \lambda_2 - \left(\frac{\Phi_f}{k_f}\right)\lambda_1\lambda_2 - k_f - k_{IC} \quad \text{(Eq. S4a)}$$

$$k_{-CS} = \frac{\lambda_1\lambda_2}{k_{CS}}\left(\frac{\Phi_f}{k_f}\right)\left[\left(1 - \frac{1}{\phi_f}\right)k_f + k_{IC} + k_{CS}\right] \quad \text{(Eq. S4b)}$$

$$k_{CR} = \lambda_1 \lambda_2 \left(\frac{\Phi_f}{k_f}\right) - k_{-CS} \qquad \text{(Eq. S4c)}$$

The forward and reverse SB-CS rate constants can then be used to determine the equilibrium constant *K* and the driving force for SB-CS are given by:

$$K = \frac{k_{CS}}{k_{-CS}} \qquad \text{(Eq. S5a)}$$

$$\Delta G_{CS} = -k_B T \ln K = -k_B T \ln\left(\frac{k_{CS}}{k_{-CS}}\right) \qquad \text{(Eq. S5b)}$$

6. Additional Crystal Views

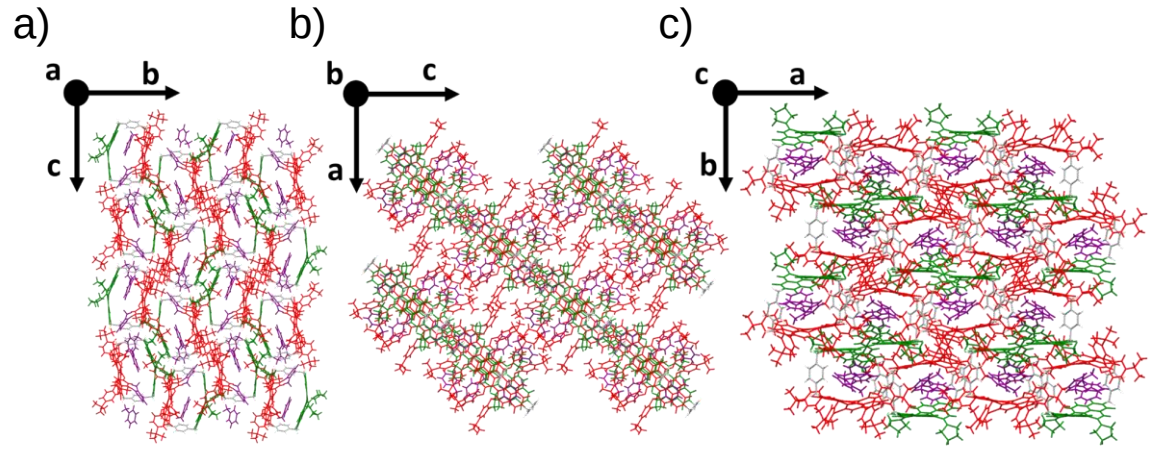

Figure S12. Viewing the extended packing of the crystal along the a) *a*-axis b) *b*-axis and c) *c*-axis of the unit cell.

7. References

1. A. F. Coleman, M. Chen, J. Zhou, J. Shin, Y. Wu, R. M. Young and M. R. Wasielewski, *J. Phys. Chem. C*, 2020, **124**, 10408-10419.
2. A. S. Lukas, Y. Zhao, S. E. Miller and M. R. Wasielewski, *J. Phys. Chem. B*, 2002, **106**, 1299-1306.
3. B. Rybtchinski, L. E. Sinks and M. R. Wasielewski, *J. Am. Chem. Soc.*, 2004, **126**, 12268-12269.
4. O. V. Dolomanov, L. J. Bourhis, R. J. Gildea, J. A. K. Howard and H. Puschmann, *J. Appl. Crystallogr.*, 2009, **42**, 339-341.
5. G. Sheldrick, *Acta Crystallographica Section A*, 2015, **71**, 3-8.
6. R. M. Young, S. M. Dyar, J. C. Barnes, M. Juricek, J. F. Stoddart, D. T. Co and M. R. Wasielewski, *J. Phys. Chem. A*, 2013, **117**, 12438-12448.
7. C. Lin, T. Kim, J. D. Schultz, R. M. Young and M. R. Wasielewski, *Nat. Chem.*, 2022, **14**, 786–793.
8. M. L. Williams, I. Schlesinger, R. M. Jacobberger and M. R. Wasielewski, *J. Am. Chem. Soc.*, 2022, **144**, 18607-18618.